Journal of the Korean Society of Oceanography
Vol. 37, No. 3, pp. 91 — 107 September 2002

A Numerical Study on the Wintertime Upwind flow of the Yellow Sea in an Idealized Basin

KYUNG TAE JUNG[1]*, CHANG WOOK PARK[2], IM SANG OH[2], HO JIN LEE[3], HYOUN WOO KANG[4]
[1]*Korea Ocean Research and Development Institute, Ansan P.O. Box 29, Seoul, Korea*
[2]*Seoul National University, Seoul 151-741 Korea*
[3]*RIAM, Kyushu University, Fukuoka, Japan*
[4]*IPRC/SOEST, University of Hawaii Honolulu, U.S.A.*

The wintertime upwind flow in the Yellow Sea has been investigated through a series of two-dimensional numerical experiments in an idealized basin. A total of 10 experiments have been carried out to examine the effects of wind forcing, bottom friction and the presence of oceanic currents sweeping the shelf of the East China Sea. A spatially uniform steady and periodic wind stresses are considered along with comparison of linear and quadratic formulations. The wind-driven flow in the absence of oceanic current has been computed using Proudman open boundary condition (POBC), while the wind-driven current in the presence of oceanic current has been computed using Flather's radiation condition (FOBC). The oceanic currents to be prescribed at the open boundary have been simulated by specifying uniform sea level gradients across the Taiwan Strait and the eastern ECS shelf. Calculations show that, as seen in Lee *et al.* (2000), oceanic flow little penetrates into the Yellow Sea in the absence of wind forcing unless a unrealistically low rate of bottom frictional dissipation is assumed. Both steady and time-periodic wind stresses invoke the upwind flow along the central trough of the Yellow Sea, independently of the presence of the oceanic current. The presence of oceanic currents very marginally alters the north-south gradient of the sea surface elevation in the Yellow Sea. Changes in the intensity and direction of the wind-induced mean upwind flow are hardly noticeable in the Yellow Sea but are found to be significant near Cheju Island where the gradient is reduced and therewith contribution of Ekman transport increases. In case of steady wind forcing circulation patterns such as two gyres on the slope sides, a cyclonic gyre on the western slope and an anticyclonic gyre on the eastern slope persist and the upwind flow composes part of the cyclonic gyre in the Yellow Sea. While in case of the time-periodic wind stress the appearance and disappearance of the patterns are repeated according to the time variation of the wind stress and the upwind flow accordingly varies with phase delay, mostly intensifying near the time when the wind forcing is approximately near the middle of the decaying stage.

Key words: Yellow Sea, Upwind flow, Oceanic current, Wind stress

INTRODUCTION

The problem of the wintertime upwind flow (northward flow) along the trough of the Yellow Sea (YS), has long attracted the considerable interest of researchers. Since the current observations by Hsueh (1988) and the two-dimensional model study by Hsueh *et al.* (1986) confirmed its presence, researches on the matter have continued in basins of both simplified and real geometry. Both analytical and numerical models have been constructed. Park (1986) first proposed a simple analytical channel model of inifinite length for the mean upwind flow. An attempt to explain the upwind flow and sea level fluctuations was made by Hsueh and Pang (1989) on the basis of coastally-trapped long wave theory. The upwind flow events were reasonably well reproduced but the model had a limitation in that an infinitely long channel was again assumed. Seung (1995) constructed a numerical model of infinite and semi-infinite channel models

*Corresponding author: ktjung@kordi.re.kr

for the mean upwind flow, focusing the effects of Shandong Peninsula on the generation of up-slope currents in the YS. These two models implicitly assumed that the mean upwind flow is formed along the central trough, compensating the wind-driven southward flows on both sides of the YS. That is, the constraint of zero cross-sectional flux was imposed at the outset. In these studies oceanic flows on the East China Sea (ECS) was neglected. Wang and Yuan (1988) carried out numerical simulations in an idealized basin with various combinations of model forcings which include the steady uniform wind stress, oceanic inflow-outflow and the baroclinic gradient due to horizontal change in temperature, and claimed that the upwind flow (called Yellow Sea Warm Current, though its definition is still arguable) is formed under the action of strong northerly winds; the higher the wind speed, the stronger the upwind current; when the northerly winds weaken or vanish, the upwind flow changes its direction, or ceases to exist. However, the basis of their conclusion was rather uncertain and evidences were revealed showing that their calculations were suffered from undesirable behaviors in the solutions associated with open boundary treatments. Furthermore, the bottom stress was represented in a quadratic form, neglecting strong tidal currents. Takahashi *et al.* (1995) examined the wintertime circulation of the YS with emphasis on topographic effects, but the idealized basin itself was far different from reality, and the bottom friction was neglected. Oceanic flows on the ECS was again neglected. Studies in basins of real topography include Choi (1982), Choi and Suh (1992) and Lee (1995). Choi (1982) and Choi and Suh (1992) considered a steady uniform wind stress, while Lee (1995) further examined the wind-driven circulations subject to a time-periodic wind forcing. These studies however all neglect the presence of oceanic current in the ECS shelf.

This study has been carried out to gain more knowledge on the wintertime circulation in the YS, particularly with regards to the role of the bottom friction as well as the presence of oceanic flows originated from Taiwan Warm Current. For numerical calculations, we have adopted the two dimensional version of POM (Princeton Ocean Model) with addition of linear bottom friction. The model basin considered has been hatched from the idealized basin devised by Seung (1995) but the coastline and the bottom topography are represented in more realistic forms especially in that Okinawa Trough is considered and the eastern side of the model domain is partly bounded by an open boundary. It is assumed that oceanic flows sweeps over the ECS shelf, entering into the domain through Taiwan Strait and flowing out of the domain through the eastern ECS shelf. The Kuroshio main stream is however omitted. At the sea surface both steady and periodic uniform wind stresses are applied. For the bottom frictional dissipation, a linear form has been basically used although a quadratic friction formulation is also employed for comparison.

MODEL

Basic model and boundary conditions

Numerical experiments have been carried out using a two-dimensional depth integrated model, more precisely, using the two-dimensional version of Princeton Ocean Model (POM) on Cartesian coordinates. Therefore, governing equations of primitive form have been used instead of the stream function formulation employed by Seung (1995). For detailed descriptions, see Mellor (1998).

A change is made on the form of bottom friction. Since we are dealing with secondary flows, which are significantly weaker than tidal currents, we employ a linear formulation, that is,

$$(\tau_{bx}, \tau_{by}) = \rho k_l (u, v) \tag{1}$$

where k_l is a linear bottom frictional coefficient with unit *m/s* and (u, v) are the components of horizontal current.

For the comparison purpose, we use a quadratic friction given by

$$(\tau_{bx}, \tau_{by}) = \rho k_q (u^2 + v^2)^{1/2} (u, v) \tag{2}$$

where k_q is a dimensionless bottom frictional coefficient.

On the coastal boundaries, the normal component of horizontal current vector (u, v) is taken to be zero.

We take, on the open part of the boundary, a radiational condition in the form

$$u - u_p = \frac{\sqrt{gh}}{h}(\zeta - \zeta_p) \tag{3}$$

where g is gravitational constant, h is water depth, u_p, ζ_p are values to be prescribed estimates at the open boundaries. The open boundary condition (3) was originally developed by Flather (1976). Wright

et al. (1986) noted that (3) allows outward propagation of disturbances deviating from u_p and ζ_p in the form of gravity waves and, in addition, development of geostrophically balanced mean elevation field along the open boundary. In the case of $u_p=\zeta_p=0$, (3) reduces to a free radiation boundary condition (Bowden, 1983) and we hereafter call it Proudman open boundary condition (POBC). For the case of non-zero values of u_p and ζ_p we hereafter call (3) Flather's open boundary condition (FOBC). The values of (ζ_p, u_p) are normally expressed by the linear sum of the contributions by wind forcing (ζ_w, u_w) and mean current (ζ_m, u_m). In that case (3) reduces to

$$u-u_m-u_w=\frac{\sqrt{gh}}{h}(\zeta-\zeta_m-\zeta_w) \tag{4}$$

In our experiments (ζ_w, u_w) are set equal to zero. The detailed procedure of prescribing the values of (ζ_m, u_m) are described later.

Model basins

Fig. 1 shows the study area and the idealized model basin. The Bohai Sea and the northern Yellow Sea are included in the northern part. At the top of the YS, Shandong Peninsula and Ongjin Peninsula are introduced as thin impermeable barriers. The coastline of the YS on the Chinese side is represented by a straight line, while on the eastern side by an irregular coastline representing Korean Peninsula. In the ECS the coastline is represented by a straight line in the western part, open on the east. Okinawa Trough and Taiwan Strait is also considered. The width of the YS is assumed to be 540 km (=B), and the length of the basin to the longitudinal direction is chosen as about 1600 km. For clarity, E1 is used to denote the eastern ECS shelf open boundary (from the southern coast of Korea to the south up to the depth of 200 m), E2 the eastern open boundary across the deep trough, while S1 denotes the southern open boundary across Taiwan Strait and S2 the southern open boundary east of Taiwan.

As in Seung (1995), the bathymetry of the YS is approximated by a central trough parallel to longitude with side slopes, a mild western slope on Chinese side and a steep eastern slope on Korean side. Slight changes have been however made. In detail, the minimum depth at the coastal sides is chosen as non-zero value, and

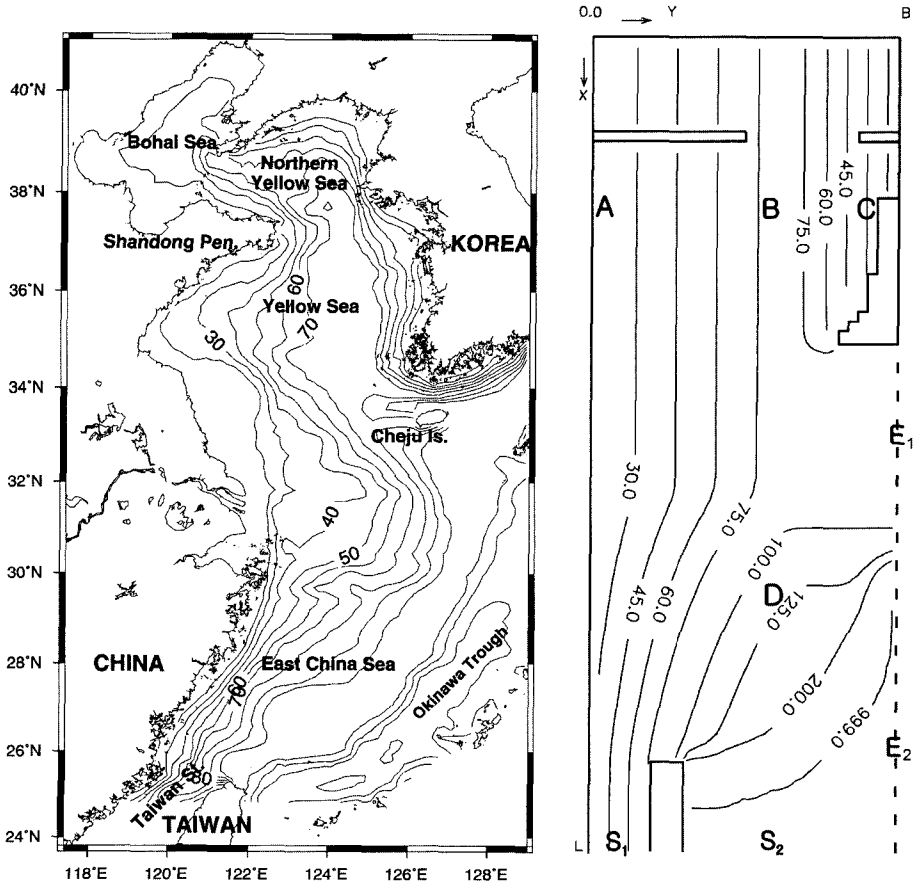

Fig. 1. The topography of the study area (left) and a simplified model basin (right).

wider regions are allocated for the trough in the YS. The maximum depth along the trough is chosen as 80 m, and the minimum depth at the Korean side 10 m, while 17 m on the Chines side. At the southern end of the domain which represents Okinawa trough the depth is assumed to be 1000 m depth.

At points A, B and C, time variations in the sea surface elevation and upwind and downwind currents are to be compared in experiment with time-periodic wind forcing, while at point D time variation in the sea surface elevation is checked for the model convergence in experiment with a steady wind forcing.

MODEL APPLICATIONS AND RESULTS

Starting from the state of no motion, the model runs have continued over a month. Time step is chosen as 6 seconds. The grid size is taken as 18×18 km. The Coriolis parameter is chosen as 0.0001. The horizontal eddy viscosity is calculated using Smagorinsky formula with its coefficient 0.2 (see Mellor, 1998). All figures are attained about 30 days of real time. The current vectors are drawn in every two grid points to x-direction. The sea surface elevation is displayed in unit of *cm*.

Initially, an experiment for steady wind-driven flows in the basin considered by Seung (1995) has been carried out for comparison purpose. We then start a set of calculations in the newly designed basin. We first elaborate, as a preliminary run, the simulation of oceanic current induced by the inflow and outflow, giving details of the methodology of determining the open boundary conditions. Then, we describe the calculations with steady and time-periodic wind stresses in the absence/presence of oceanic flows.

The steady wind stresses are imposed as:

$$\tau_{sx} = 0.05\ N/m^2,\quad \tau_{sy} = 0.0 \tag{5}$$

while, for the time-periodic wind stress,

$$\tau_{sx} = 0.05 - 0.05\cos(\omega_w t),\quad \tau_{sy} = 0.0 \tag{6}$$

where $\omega_w = 2\pi/T_w$, and T_w the period of wind variation is chosen to be 4 days as in Takahashi *et al.* (1995). Note that the wind stress takes a positive value when the northerly wind acts (we chose positive x to the south). The wind stress (unit in N/m^2) is however larger than that used by Takahashi *et al.* (1995) by about 28%.

For the calculations with the linear bottom friction we take

$$k_l = 0.002 \text{ m/s} \tag{7}$$

while, for the calculations with the quadratic bottom friction, we take

$$k_q = 0.0025 \tag{8}$$

Comments are here made on the background of choosing the value of k_l. In the literature use of a bottom stress of quadratic form is usual and the value given in (8) is commonly accepted. It should be however noted that (8) may be chosen only for dominant flows. In case of the YS tidal currents are omnipresent so that the enhancement of bottom friction due to tidal current must be somehow accounted for. Since the oceanic flows (and even wind-driven flows) are relatively weak flows superimposed on strong tidal currents, it is appropriate to use a linear formula for the bottom friction. According to Hunter (1975), the effective linear bottom friction coefficient experienced by a steady flow in the presence of tidal flow is given by the formula.

$$k_l = \frac{4\hat{u}_T}{\pi} k_q \tag{9}$$

where $\hat{u}_T$ is the amplitude of depth-mean tidal currents. For YS values of $\hat{u}_T$ range 0.5 m/s to 1 m/s. Then, we are led to the values of k_l=0.0016-0.0032 m/s. The final value 0.002 m/s is same as that used by Seung and Shin (1996).

In this study use of the linear bottom friction therefore represents calculations to account for tidal stirring effects, while use of the quadratic friction represents calculations to neglect the effects of strong tidal currents. For the use of linear bottom friction in modeling secondary flows in a tide-dominated region, see Wright *et al.* (1986) and Ladner and Das (1991).

Brief description on the wind-driven circulation considered in the idealized basin considered by Seung (1995)

In this case the lateral boundary is bounded by straight coastlines, and Okinawa Trough is absent. POBC has been applied to the southern boundary. The bottom friction is represented in a linear form. We could see (results not shown) that the circulation patterns are in good agreement with each other, showing the upwind flow with slightly biased to the western slope of the trough, the formation of southward flows along the both sides of the lateral channel boundary. Features discussed by Seung (1995) such as a broad up-slope flow below Shandong Peninsula, thin up-slope

and broad down-slope flows below Ongjin Peninsula and the upwind flow along the trough appear.

Preliminary model runs for determination of open boundary conditions for oceanic flows

For these calculations, it is assumed at the outset that the flow system sweeping the ECS shelf is formed by the inflow through Taiwan Strait (S1) and the outflow through the eastern shelf seas (E1) of the ECS. The Kuroshio main stream over the Okinawa Trough are omitted.

The elevation associated with oceanic flow, ζ_m, along the open boundary is determined in the following way. We first guess values of the gradient of sea surface elevation along the open boundaries at Taiwan Strait, that is, $\zeta_{m,y}$ at S1, and the eastern ECS shelf, $\zeta_{m,x}$ at E1 (subscripts x, y denote partial derivatives). Then, we interpolate spatially, setting ζ_m=0, in case of the eastern ECS at the point near the shelf edge, in case of Taiwan Strait at the western end of the strait; in the rest part of the open boundaries (S2 and E2) values of ζ_m are initially set equal to zero. We then carry out a model run with an elevation-specified condition and store the final velocity outputs along open boundaries as u_m (or v_m) for the later experiments with radiation condition (4) under wind forcing plus oceanic flows. In calculating u_m or v_m we have taken averages of the two values defined at the open boundary cells. Since $\zeta_w=u_w=v_w=0$ is assumed throughout the calculations, the stored values ζ_m, u_m and v_m are time-invariant and coincide with ζ_p, u_p and v_p.

Table 1 summarizes the details of the imposed sea surface elevation gradient at Taiwan Strait (S1) and the eastern ECS shelf region (E1). The associated total volume transports across the open boundaries are included together.

The prescribed inflow volume transports at Taiwan Strait are approximately half of that given by Lee *et al.* (2000), while the prescribed outflow volume transport is by about 50% larger than that given by Lee *et al.* (2000) at Korea Strait. It should be noted that the balance between the inflows through Taiwan Strait and the outflows through the open boundary of the eastern ECS shelf sea is not compulsorily needed. Furthermore, although the imposed sea level gradients are same, it is seen that the volume transports for the linear friction case (Exp. L1) are smaller than that of the quadratic friction case (Exp. Q1). Oceanic flow fields for linear and quadratic frictions are presented in Fig. 2. Discussions on the fields are for convenience to be made below.

Steady wind-driven flow in the absence of oceanic flows

Fig. 3 shows the wind-driven flows computed with the steady uniform wind stress for the linear (Exp. L2) and quadratic frictions (Exp. Q2), while neglecting the oceanic currents in the ECS shelf. POBC has been applied to all open boundaries, assuming that $\zeta_p=u_p=v_p=0$.

It is evident that the model responses are markedly different according to the bottom frictional formulation. The high energy dissipation by use of the linear friction produces weak flows throughout the domain, while the low energy dissipation by use of the quadratic bottom friction invokes comparatively strong flows. The associated sea level distributions are also different; the linear bottom friction tends to smooth out the spatial variation in sea surface elevation, while the quadratic bottom friction produces considerable spatial gradients in sea surface elevation, inducing stronger currents. Oscillations in the results with the quadratic bottom friction near the shelf edge of the ECS attribute to the low rate of bottom frictional dissipation.

Despite the difference in flow intensity, the overall features of circulation in the Bohai Sea, the northern Yellow Sea and the YS are not much different; Both the linear and quadratic frictions produces a northward flow along the deep trough of the YS, southward flows along the Chinese coast with broad width, and an anti-cyclonic gyre over the eastern YS and the northern YS. The presence of Shandong Pen-

Table 1. Summary of sea level gradients and volume transports specified for oceanic flows

Cases	Bottom friction	Taiwan Strait (S1)		eastern ECS shelf sea (E1)	
		$\frac{\partial \zeta_m}{\partial y}$	$\int H u_m dy$	$\frac{\partial \zeta_m}{\partial x}$	$\int H v_m dx$
Exp. L1	Linear	0.1625×10^{-5}	−0.94 Sv	0.4333×10^{-5}	2.47 Sv
Exp. Q1	Quad.	0.1625×10^{-5}	−1.26 Sv	0.4333×10^{-5}	2.65 Sv

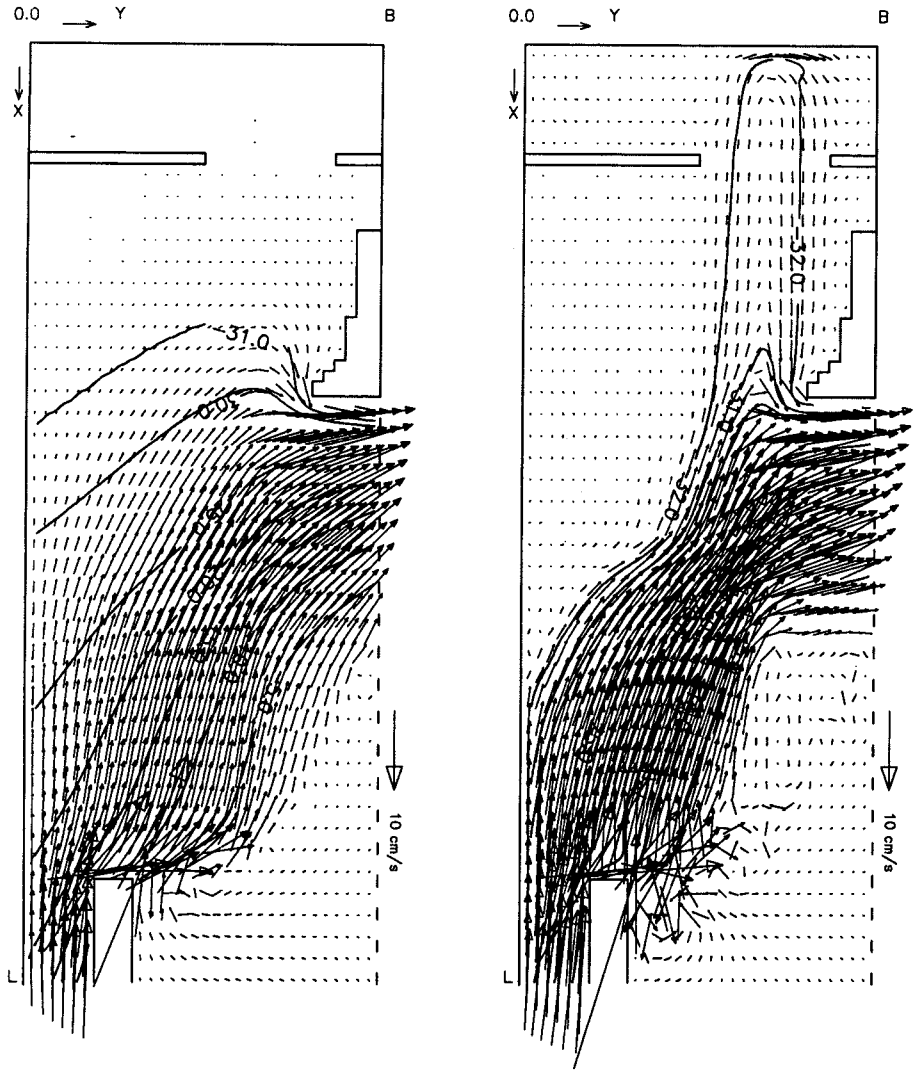

Fig. 2. Oceanic current computed by enforcing sea level gradients at the open boundaries at Taiwan Strait and the eastern East China Sea shelf: with linear (left: Exp. L1) and quadratic bottom friction (right: Exp. Q1).

insula commonly develops, though its intensities are quite different depending upon the type of bottom friction, westward up-slope flows over the YS, extending up to the point of the ECS where the depth variation to the x-direction occurs (that is, near 30°N). Near the top of the northern YS, eastward up-slope flows are developed with thin thickness. Seung (1995) explained the difference in terms of vorticity balance, saying that, on the western slope of the YS below Shandong Peninsula the vorticity due to vortex shrinking and the wind stress torque is balanced out, while on the eastern slope of the YS (in this study the northern YS) the vorticity balance between the two is not achieved.

Differences in the circulation patterns are noticeable in the ECS. In case of the linear friction the influx across the eastern open boundary contributes to the formation of the upwind flow in the YS, while in case of the quadratic friction the upwind flows are apparently extended up to the northern Taiwan with a similar width and three branches, the first separated from the southward flow on the Chinese side, the other two invoked at both sides of Taiwan, contribute to the development of the upwind flows.

Comments on the flows in Taiwan Strait are worthwhile. It is noted that the linear friction produces southward flows in the Taiwan Strait which is almost parallel to the coastline. On the contrary, the quadratic friction invokes a narrow northward flow which is opposite to the direction of wind forcing and, furthermore, unrealistic flows are formed at the grid points near the open boundary. Calculations reveal that the formation of the counter current depends upon the width of the strait (results not shown). As the width of the strait increases the width of the northward flow on the western side of Taiwan increases, while, as the width of the strait decreases, the northward flow and the unrealistic behaviour at

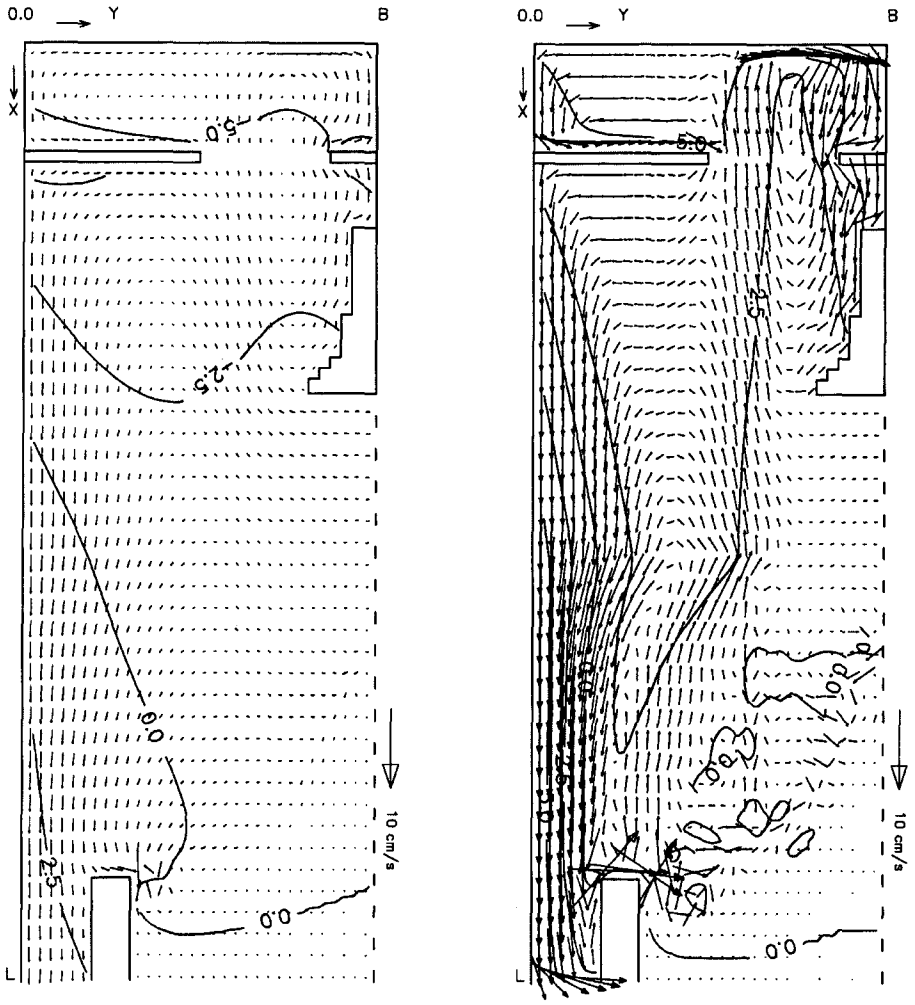

Fig. 3. Wind-driven current computed by the steady uniform wind stress in the absence of oceanic current with: linear (left: Exp. L2) and quadratic frictions (right: Exp. Q2).

the open boundary grid points gradually tend to disappear. The incorrect steady state response obtained using POBC was shown in Palma and Matano (1998) in a wind-driven spin-up experiment in a zonal channel with a sloping bottom, and also Hayashi et al (1986), who related the problem to physical incompatibilities between the scheme and the proper solution at the open boundaries. It is seen that use of a linear friction lessens the abnormal tendency.

Steady wind-driven flows in the presence of oceanic flows

Fig. 4 shows flow fields computed with the steady uniform wind stress as well as the oceanic inflows-outflows for the linear (Exp. L3) and quadratic frictions (Exp. Q3). FOBC has been applied to all open boundaries.

Comparing with Figs. 2 and 3, it is seen that combined features of circulation shown in Exp. L1 and L2, and Exp. Q1 and Q2 appear. Both the linear and quadratic frictions produces a northward flow along the deep trough of the YS, southward flows along the Chinese coast with broad width, and an anti-cyclonic circulation over the eastern YS and the northern YS. The westward up-slope flows and southward coastal currents characterize the circulation on the western slope of the YS, while near the northern end of the northern Yellow Sea, the eastward up-slope flows with thin thickness and an anti-cyclonic gyre are noticeable. In the ECS shelf oceanic flows overwhelmingly appear. On the western slope region of the ECS, the southward coastal current and the northward oceanic current impinge each other. Consequently, the southward flows rapidly becomes narrower, merging with the oceanic flows. In Taiwan Strait the oceanic inflows are apparently weakened. The quadratic friction allows the wind-driven coastal flow to go farther southward up to the top of the strait than the linear friction does. Calculations with reduced inflow trans-

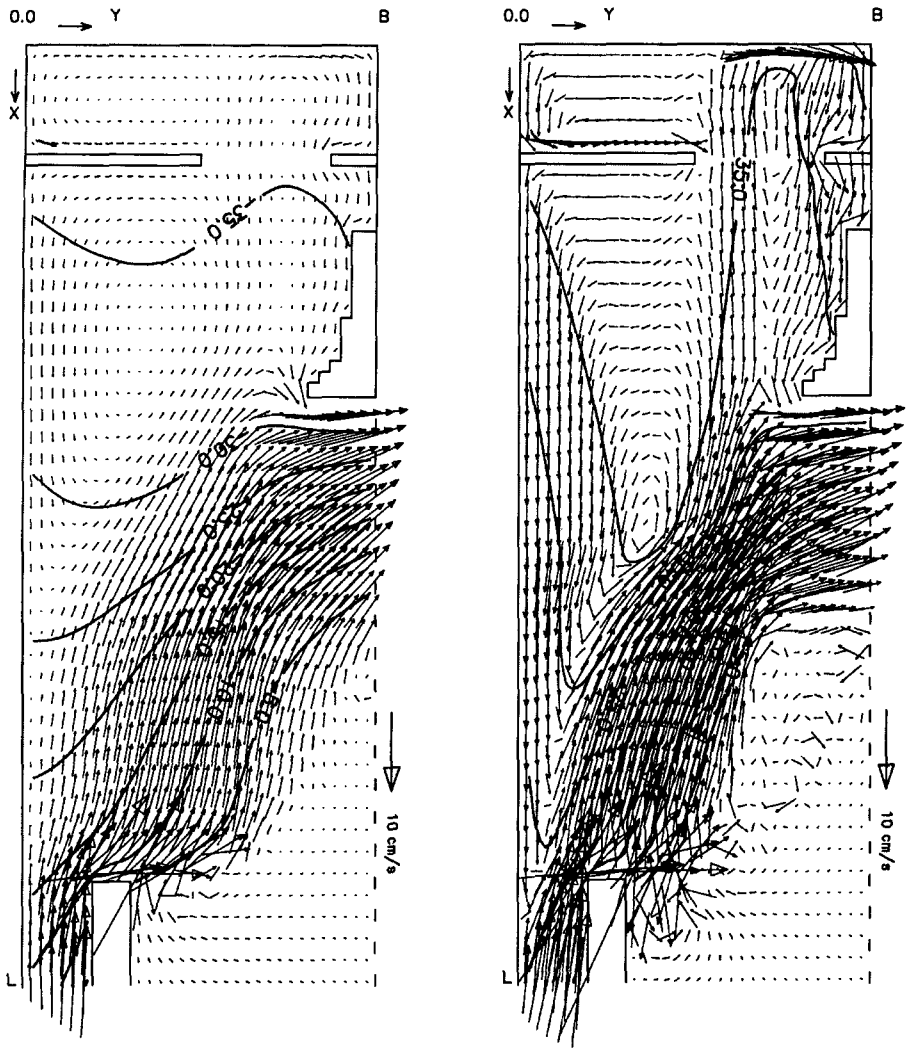

Fig. 4. Wind-driven current computed by the steady uniform wind stress in the presence of oceanic current with: linear (left: Exp. L3) and quadratic frictions (right: Exp. Q3).

ports (not shown) indicate that with, in case of linear friction, the southward wind-driven flow hardly penetrates up to the bottom of the model domain unless the wind stress is increased and/or the outflow transport on E1 is reduced. It is also interesting to note that considerable fluctuations occur east of Taiwan, particularly for the case of quadratic friction.

Comments on differences in the circulation patterns between the linear and quadratic frictions are of value. Calculations show that the linear friction develops the oceanic flow over the entire shelf sea region of the ECS, while the quadratic friction develops flows more closely following isobars less than 125 m. Strong bottom friction induces the flows crossing isobars at substantial angle. Neglecting the wind driving force, the steady state vorticity balance is approximately given by (Lee *et al.*, 2000):

$$\frac{f}{h}\hat{u}\cdot\nabla h = -\hat{k}\cdot\nabla\times\frac{\hat{\tau}_b}{h} \tag{10}$$

where f is the Coriolis parameter, $\hat{u}$ the current vector, $\hat{k}$ is the unit vector in the vertical direction, and hat $\hat{\tau}_b$ are stress vectors at the sea surface and bottom, respectively. Equation (10) indicates that controls the flow field, more precisely, the volume transport to the cross-isobaric direction and the angle between the isobaric contours and local flow direction. We note that use of the quadratic friction with k_q=0.0025 obviously underestimates the bottom friction, by about one order comparing with that computed with linear friction with k_l= 0.002 m/s, so that $\hat{u}\cdot\nabla h$ goes to nearly zero. In that case, the flow tend to follow isobaric contours. On the while, use of the linear friction increases the value of the right hand side of (10) and therewith the flow tends to cross over isobars with certain angles.

Further comments are given on the formation of an anti-cyclonic gyre on the eastern slope of YS and the northern YS. In the results shown in Jung *et al.* (2001), two gyres appeared, an anti-cyclonic gyre off

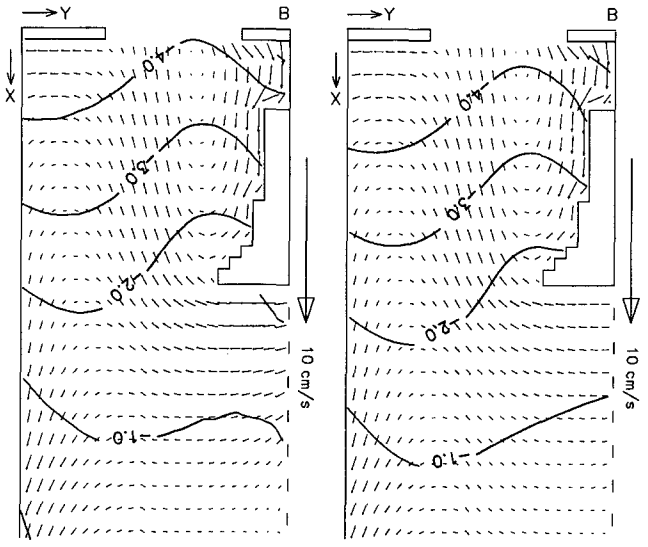

Fig. 5. A comparison of wind-driven currents in the YS in the absence and presence of oceanic flow computed using linear friction (left: Exp. L3 - Exp. L1. right: L2).

Kyunggi Bay and a cyclonic gyre in the northern YS. This attributes to the difference in topography and external forcings (in Jung *et al.* (2001), M2 tide, monthly mean non-uniform wind stresses and baroclinic forcing were included).

For the close examination of influence of oceanic flow upon the upwind flow, the wind induced flow field in the YS deduced by subtracting results from Exp. L1 from Exp. L3 have been compared with results from Exp. L2 (Fig. 5). It is seen that the intensity and directions of the upwind flow and the southward wind-driven currents on both Chinese and Korean coasts are very marginally little changed despite the change in the sea surface elevation fields, more specifically, the variation in the north-south gradient of sea surface elevation. We note from Fig. 5 that the presence of oceanic flow results in the reduction of the north-south gradient by about 5%. With this change significant changes in the intensity and direction of the upwind flow in the YS can be hardly expected. There is however noticeable changes in the flows south of Korean Peninsula. The wind-induced upwind flow in the YS deduced by taking into account the interaction with oceanic flow (Exp. L3 - Exp. l) is maintained by the volume supply from relatively strong westward flows on the northen part of E1, while the wind-induced upwind flow in the YS obtained by neglecting the interaction with oceanic flow (Exp. L2) is maintained by the volume supply from the whole ECS on the side of E1. This attributes to local

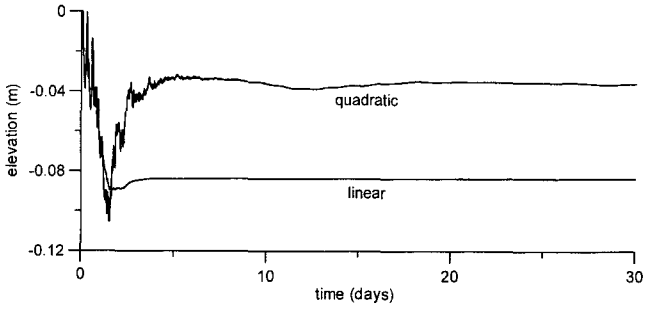

Fig. 6. Time variations in sea surface elevation at point D.

change in the sea surface elevation; the result of (Exp. L3 - Exp. L1) shows significant reduction in north-south gradient of the sea surface elevation on the northern part of E1 (the sea surface elevation contour off the southern coast of Korea denotes -1.0 cm); consequently, the westward transport across the northern part of E1 is locally increased. Neglecting bottom friction, the volume transport at steady state can be determined by

$$-fv = -g\frac{\partial \zeta}{\partial x} + \frac{\tau_{sx}}{\rho h} \tag{11}$$

Note that the positive gradient of the sea surface elevation suppresses the westward transport.

Before moving to next section, it might be worthwhile to check the model convergence. As a simple way we present in Fig. 6 time variations in sea surface elevation at point D, which is fairly close to shelf edge. As expected the spin-up times of Exp. L3 and Exp. Q3 are very much different. Despite the discrepancy in the imposed inflow-outflow velocities (and transport) as well as sea surface elevation, it is evident that the model shows no sign of instabilities or trend, confirming that the radiational boundary condition works satisfactorily.

Sensitivities of the steady model response to the change in open boundary oceanic forcing

To investigate how the intensity of oceanic flows affects the circulation, we have carried out experiments with systematic changes in the sea level gradient ζ_m on either Taiwan Strait or the eastern ECS. Since the volume transports across the open boundaries are changed according to the interior response, the calculations have been carried out in two steps. That is, the 1st runs to determine the u_m (and v_m) have been repeated and thereafter the 2nd runs with steady wind stress have been carried out. In these

Table 2. Summary of volume transports across the shelf open boundaries

Cases	Taiwan Strait (S1)			eastern ECS shelf sea (E1)		
	$\frac{\partial \zeta_m}{\partial y} \times 10^{-5}$	$\int Hu_m dy$	$\int Hudy$	$\frac{\partial \zeta_m}{\partial x} \times 10^{-5}$	$\int Hv_m dx$	$\int Hvdx$
Exp. L3	0.1625	−0.94 Sv	−0.86 Sv	0.4333	2.47 Sv	2.34 Sv
Exp. L4	0.1625*3.00	−2.03 Sv	−1.96 Sv	0.4333	2.52 Sv	2.38 Sv
Exp. L5	0.1625/4.00	−0.53 Sv	−0.45 Sv	0.4333	2.46 Sv	2.33 Sv
Exp. L6	0.1625	−1.34 Sv	−1.27 Sv	0.433*2.0	4.92 Sv	4.77 Sv
Exp. L7	0.1625	−0.67 Sv	−0.59 Sv	0.433/3.0	0.84 Sv	0.72 Sv

calculations the linear friction has been employed.

Table 2 summarizes the volume transports at the open boundaries along with the prescribed sea surface gradients. It is evident that increasing (decreasing) the sea surface gradient results the increase (decrease) in the prescribed volume transport ($\int|v_m|dx$ or $\int|u_m|dy$ computed initially using the open boundary condition $\zeta=\zeta_m$) which in turn produces increase (decrease) in the resultant volume transport ($\int|v|dx$ or $\int|u|dy$ computed using the radiational open boundary condition (4)). However, there is a subtle difference in the model responses between the changes in the open boundary forcings at Taiwan Strait (S1) and the eastern ECS (E1). That is, comparing the results from Exp. L3 and Exp. L4, we see that the increase in the sea surface gradient and the associated volume transport at Taiwan Strait gives rise to significant increase in the inflow volume transport (about 1.1 Sv), but little affecting the volume transport in the eastern ECS (about 0.04 Sv). On the while, comparison of Exp. L3 and Exp. L6 shows that increase in the sea surface gradient and the prescribed volume transport at the eastern ECS open boundary gives rises to increase in the outflow volume transport (about 2.4 Sv), and at the same time significantly affects the inflow volume transport at Taiwan Strait (about 0.4 Sv). This tendency is found even for the case the volume transports through S1 and E1 are initially balanced out, indicating that the deep sea region of the ECS acts to some degree as a sink for the inflow through Taiwan Strait and as a source for the outflow through the eastern ECS shelf. In that course, considerable amount of volume transports occurs across the open boundaries S2 and E2. In case of Exp. L1, volume transports through S2 and E2 are −0.81 Sv and −0.72 Sv, respectively, while in case of Exp. L3 volume transports through S2 and E2 are −0.71 Sv and −0.77 Sv, respectively. The volume transports across S2 and E2 increase as the discrepancy in the transports between S1 and E1 increases. In general the volume transport across S2 is larger than that of E2.

Brief comment is given on the difference between $\int|v_m|dx$ and $\int|u_m|dx$ at E1 (−0.13 Sv), which represents physically the effects of wind forcing and is comparable with the transport at E1 (−0.11 Sv) computed in Exp. L2. However, strictly speaking, the difference does not correspond to pure Ekman drift because the change in the distribution of sea surface elevation is invoked.

Fig. 7 displays the flow fields computed with changes at Taiwan Strait (Exp. L4 with sea level gradient three times larger than that of Exp. L3, Exp. L5 with sea level gradient one fourth of that of Exp. L3), fixing the condition at the eastern ECS, while Fig. 8 with changes at the eastern ECS (Exp. L6 with sea level gradient two times larger than that of Exp. L3, Exp. L7 with sea level gradient one third of that of Exp. L3), fixing the condition at Taiwan Strait.

From Fig. 7, we see that increasing the sea surface gradient and the prescribed inflow volume transport at the open boundary of Taiwan Strait obviously intensifies the flow and the sea surface slopes in Taiwan Strait, while decreasing the sea surface gradient and the prescribed inflow transport markedly reduces the volume transport of the inflows through Taiwan Strait. However, features of the circulation in other parts are not apparently altered except for the sea region near the northern coast of Taiwan.

From Fig. 8, we see that increasing the sea surface gradient at the eastern ECS open boundary obviously intensifies the flow and the sea surface slopes in the ECS shelf sea regions, while decreasing the sea surface gradient markedly reduces the volume transport of the inflows through Taiwan Strait, consequently breaking the flow system continuing from Taiwan Strait to the eastern ECS shelf sea. In case the oceanic flow intensifies the southward extent of the wind-driven flow along the Chinese coast is reduced and then the intensity of the upwind flow slightly

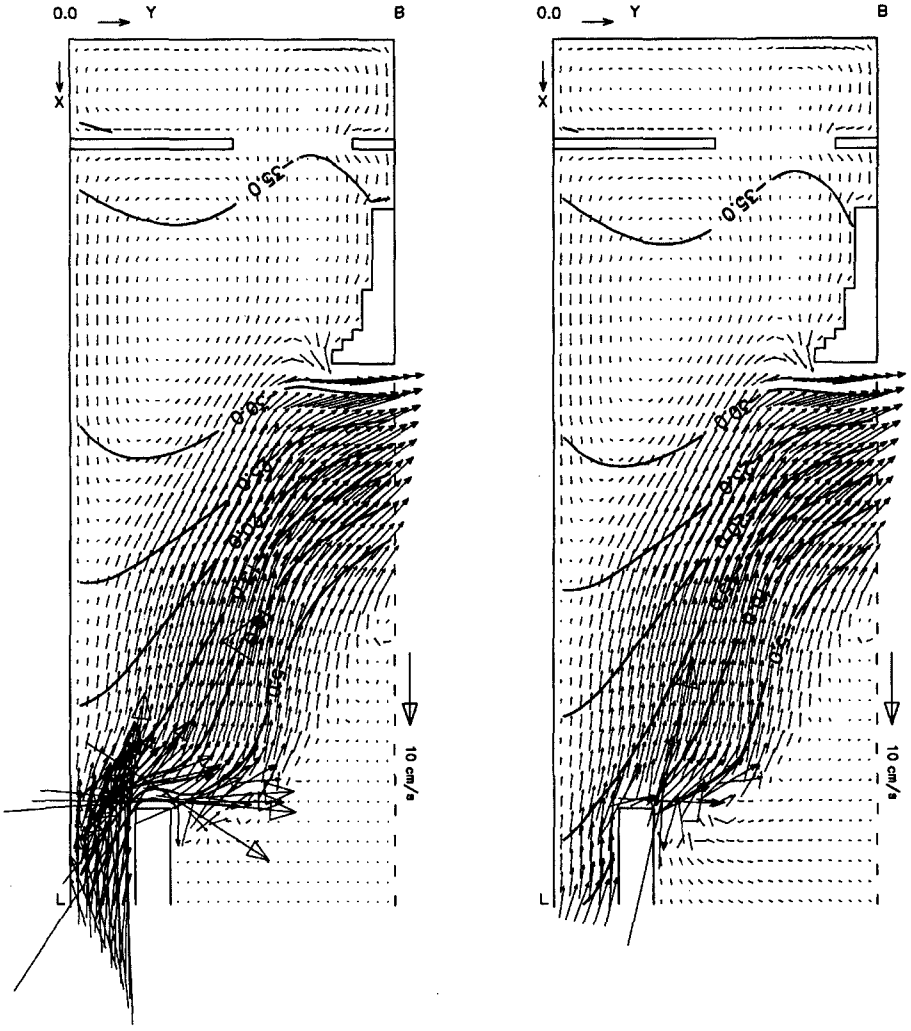

Fig. 7. Wind-driven current computed by the steady uniform wind stress in the presence of oceanic current with changes in the sea level gradient at the open boundary of Taiwan Strait using linear friction (left: L4, right: Exp. L5).

increases. In case the oceanic flow reduces the southward wind-driven flows along the Chinese coast overwhelms the oceanic flow and then extend up to the left top of Taiwan Strait. The central ECS in this case supplies the mass for the upwind flow. Without presenting detailed results we briefly comment on sensitivity study results. A series of calculations with further reduced inflow volume transport reveal very marginal increase in the penetration distance of the southward coastal flow into the Taiwan Strait. It is noted that increasing the wind stress allows the southward coastal flow to penetrate into the Taiwan Strait. and even to its bottom. This will be reported in the near future.

Wind-driven flows subject to the time-varying wind stress of 4 days period in the absence/presence of oceanic flows

From now we consider the response to time varying wind stress defined as in (6). The open boundary condition is identical to that of Exp. L2 in calculation without oceanic flow, while identical to that of Exp. L3 in calculation with oceanic flow. The model run continues over 34 days and the final four days results are presented.

Fig. 9 displays the snap shots of flow fields in an interval of 0.5 days ($t = nT_w - T_w/2$, $nT_w - 1/4T_w$, nT_w, $nT_w + 1/4\ T_w$, n is an integer, in radians $\omega_w\ t = -\pi$, $-1/2\pi$, 0 and $1/2\pi$) computed in the absence of oceanic current. Note that the wind stress becomes a positive maximum of 0.1 N/m^2 at $t = nT_w - T_w/2$, 0.05 N/m^2 at $t = nT_w - 1/4\ T_w$, zero at $t = nT_w$ and 0.05 N/m^2 at $t = nT_w + 1/4\ T_w$. It is evident that the formation of the upwind flows markedly vary along with the phase of wind forcing. The southward coastal current on the Chinese side intensifies when the wind stress is near the maximum (see more details in Fig. 11 to be shown). At this stage there is a weak northward flow in the YS. However, the flow is part of the anti-cyclonic

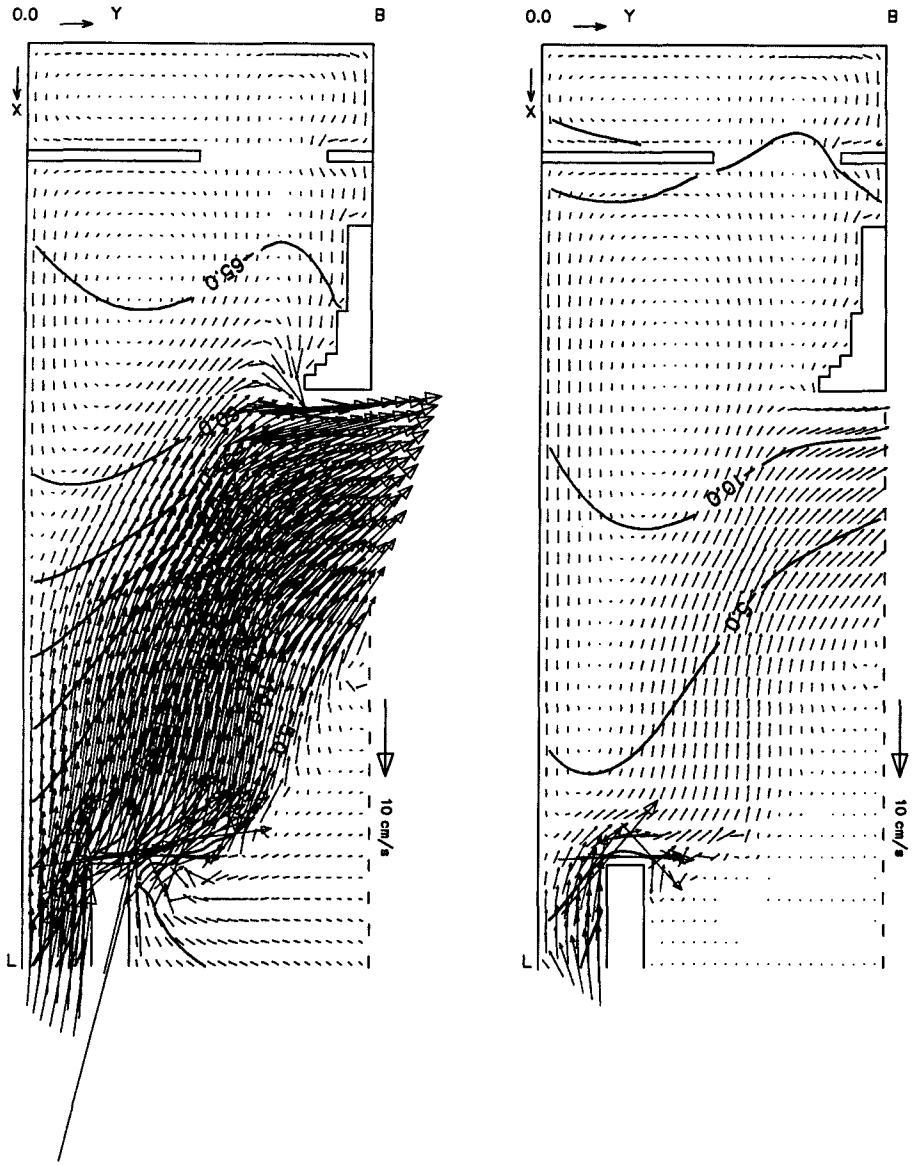

Fig. 8. Wind-driven current computed by the steady uniform wind stress in the presence of oceanic current with changes in the sea level gradient at the open boundary of the eastern East China Sea shelf using linear friction (left: L6, right: Exp. L7).

gyre in the eastern slope of the YS and the northern YS. Strong northward flows are formed at $t = nT_w$–1/4 T_w when the northerly wind is at the middle of a decaying stage. It is noted that the upwind flow develops with broader width. At this stage the southward current on the Chinese side considerably loses its intensity. At $t = nT_w$, the southward current on the Chinese side almost disappears, while the upwind flow is at the stage of losing its intensity. At $t = nT_w$+1/4 T_w, the southward current on the Chinese side is at the developing stage, while the upwind flow becomes negligibly small.

It is evident that the sea surface elevation fields and the volume flux through Taiwan Strait also vary significantly in accordance with the phase of wind forcing. Therefore, the transient upwind flow may be generated as a relaxation procedure as claimed by Hsueh *et al.* (1986). However, the upwind flow is not simply the northward flow penetrating into the YS from the ECS; near the time a positive wind maximum occurs, the upwind flow is part of the anticyclonic gyre within the YS and the northern ECS, during the decaying stage of the wind stress, it is the flow penetrating from the ECS with broad width.

Fig. 10 displays the snap shots of flow fields in an interval of 0.5 days in the presence of the oceanic current. It is seen that the computed upwind flow follows the phase of that computed in the absence of the oceanic flow and the intensity is very similar. However, difference lies in its penetration path. That is, in case when the oceanic flow is absent, the northward penetration into the YS occurs from the central

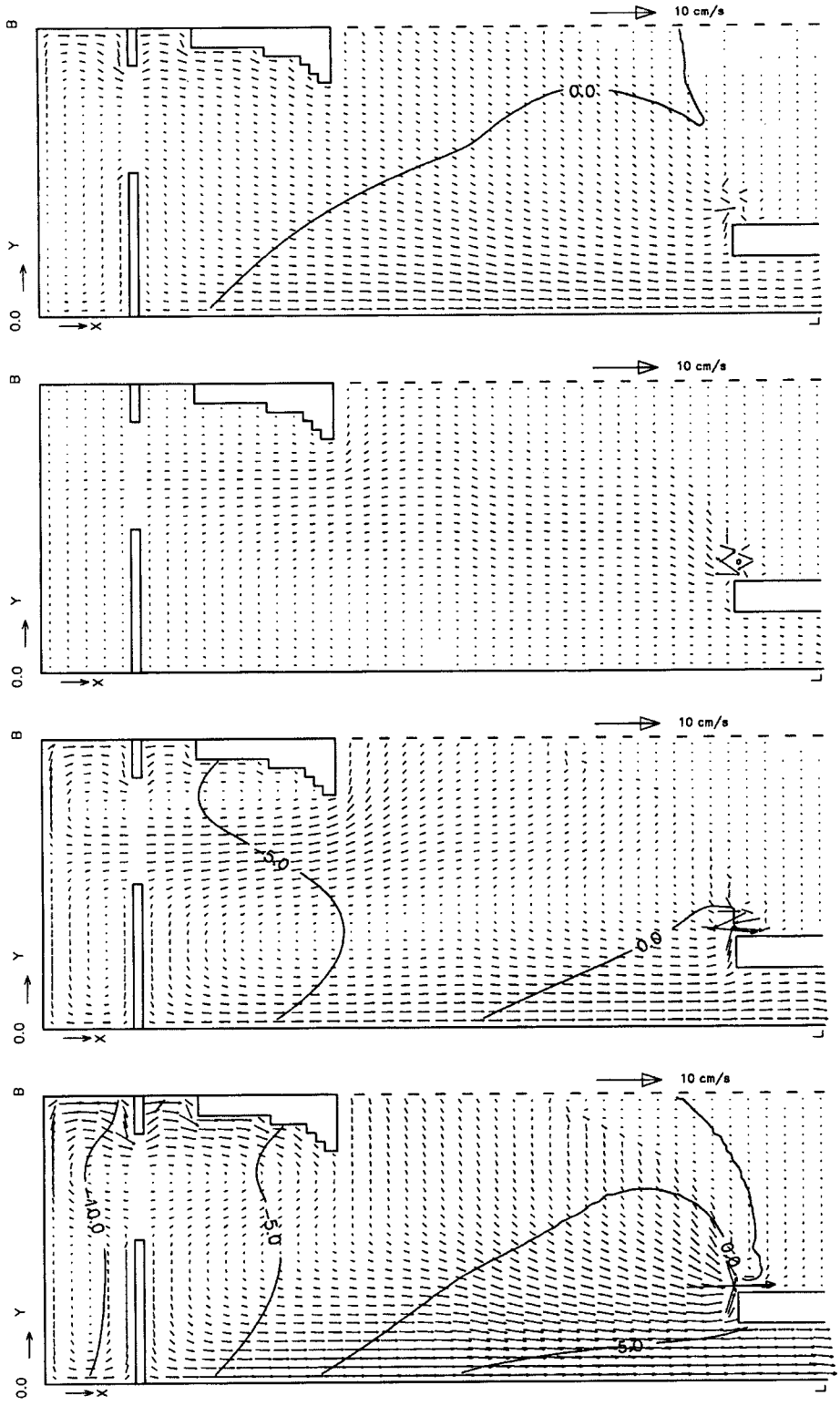

Fig. 9. Wind-driven currents at times (from left to right $\omega_w t = -\pi(\tau_{sx}=0.1\ \mathrm{N/m^2})$, $-1/2\pi$, $0(\tau_{sx}=0)$ and $1/2\pi$) computed by the time-periodic uniform wind stress in the absence of oceanic current using linear friction.

and eastern parts of the ECS, while, in the presence of oceanic flow, the northward penetration occurs over the western slope of the ECS shelf.

Fig. 11 shows time variations in wind stress, sea surface elevations and u velocities at three selected points A, B and C (see Fig. 1). It is seen that the presence of the oceanic current affects very little the time variations in the sea elevation and u velocity; only the mean values of sea surface elevation are different.

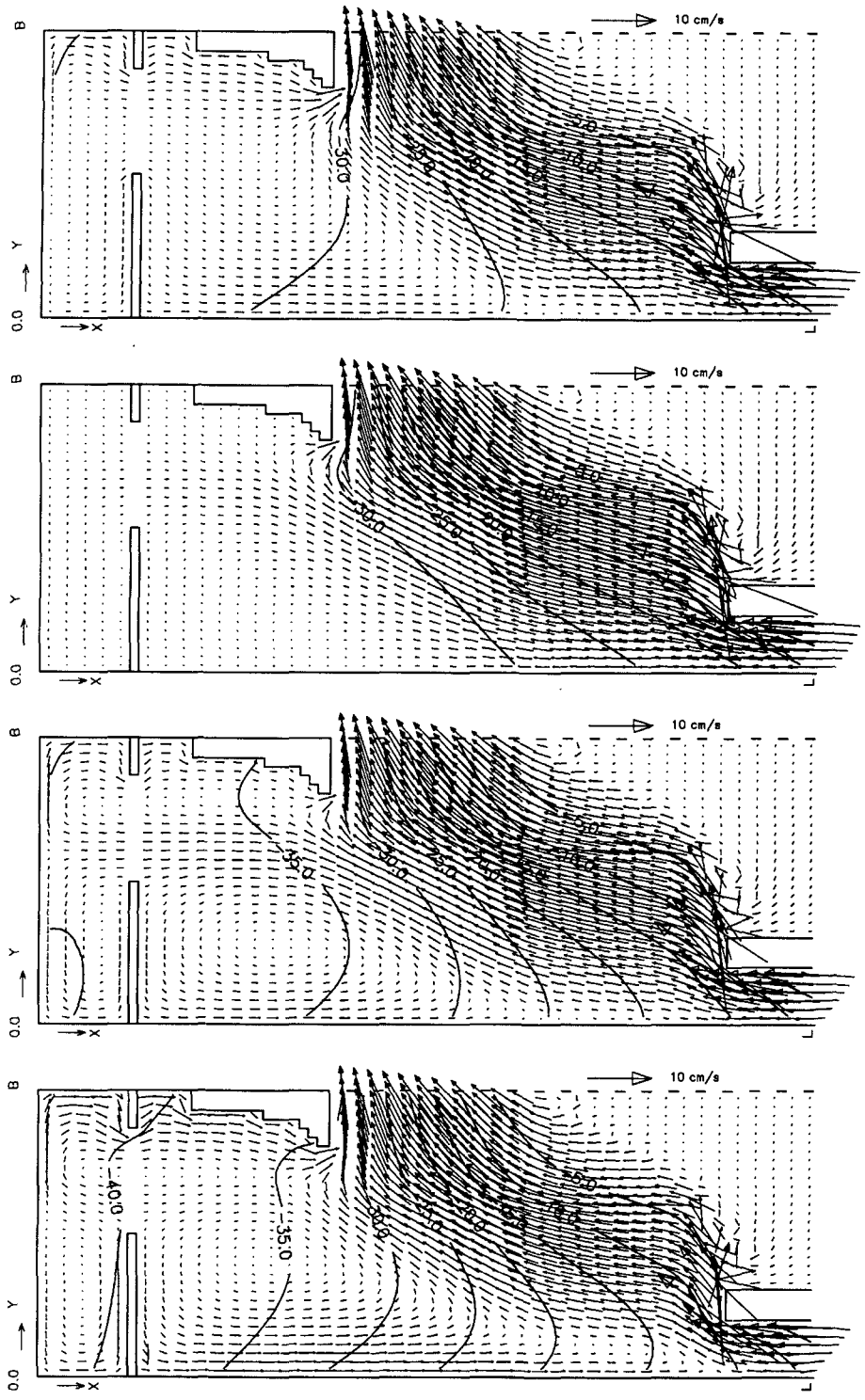

Fig. 10. Wind-driven currents at times (from left to right $\omega_w t = -\pi(\tau_{sx}=0.1\ N/m^2)$, $-1/2\pi$, $0(\tau_{sx}=0)$ and $1/2\pi$) computed by the time-periodic uniform wind stress in the presence of oceanic current using linear friction.

It is however interesting to note phase differences among wind stress, sea surface elevations and u velocities (north-south component). The set-down reaches a minimum by about 0.68 days at point A, by about 0.44 days at point B and by about 0.22 days at point C after the northerly wind maximum occurs. The maximum set-up occurs with similar values of phase delay after the wind stress goes to zero. The u velocities at point B are predominantly negative, that is against the wind stress, forming a upwind flow; the u velocities become positive for sometime near the middle of the stage when the northerly wind intensifies, forming a weak

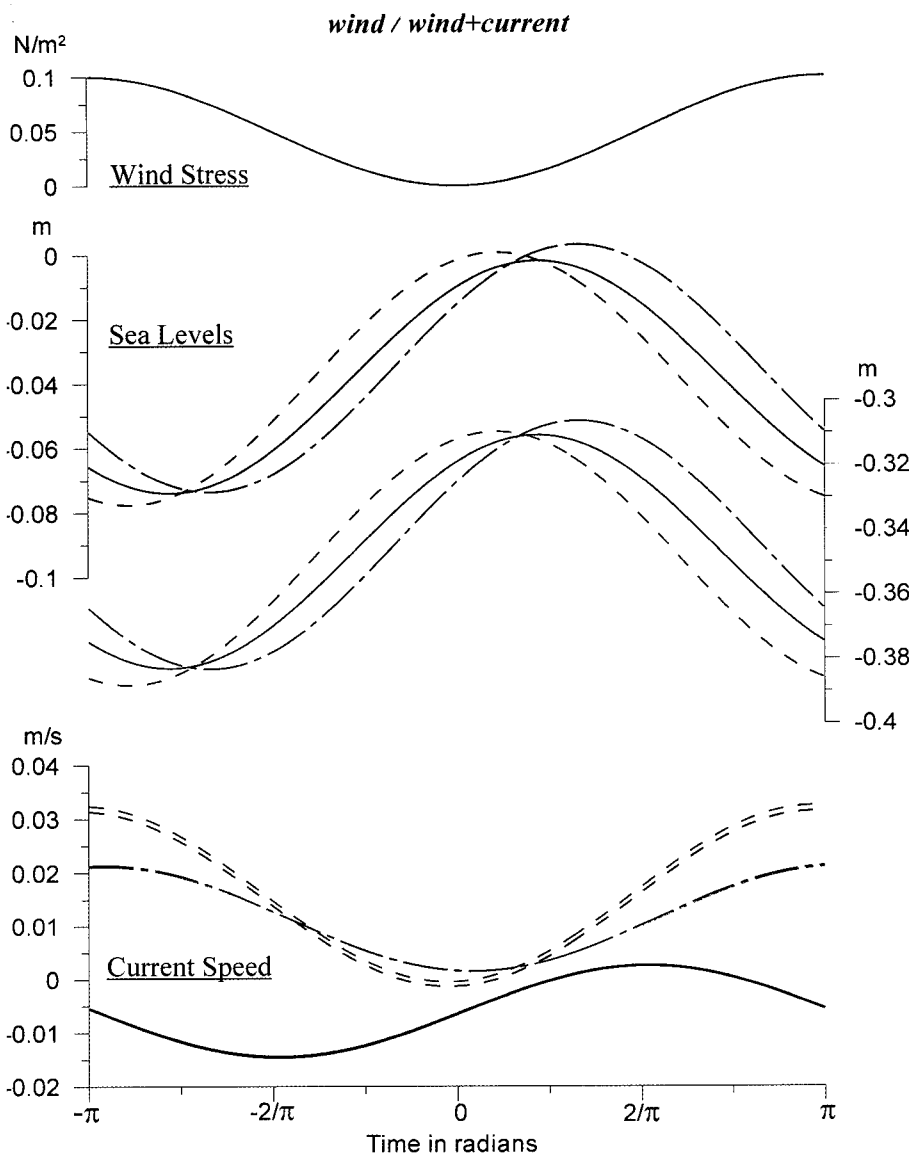

Fig. 11. Time variations in sea surface elevations and u currents (north-south components) at selected points A (dashdot line), B (solid line) and C (dashed line) computed by the time-periodic uniform wind stress in the absence(black)/presence(red) of oceanic current using linear friction.

downwind flow. At points A and C, the flows always goes southwards, that is, forming downwind flows. It is noted that the upwind current at point B reaches its maximum about one day after the wind stress maximum. The downwind flows at points A and C are almost in phase with wind stress but close examination reveals that the u velocity at point A shows a peak about 0.09 days after the wind stress maximum, at point C, 0.05 days ahead of the wind stress maximum.

CONCLUSIONS AND DISCUSSIONS

The wintertime circulation in the YS and the ECS has been numerically investigated in an idealized basin with emphasize on the formation of the upwind flows in the absence/presence of oceanic flows over the ECS shelf sea regions.

Calculations show that both steady and time-periodic wind stresses invoke the upwind flow along the central trough of the Yellow Sea, independently of the presence of the oceanic current. That is, the mean upwind flow is generated by steady uniform wind stress in the presence of oceanic flow, while the intermittent upwind flow is generated by the time-periodic uniform wind stress, independently of the presence of oceanic flow. In case of steady forcing circulation patterns such as two gyres on the slope sides, a cyclonic gyre on the western slope and an anticyclonic gyre on the eastern slope persist and the upwind flow composes part of the cyclonic gyre in the Yellow Sea. On the contrary, in case of the time-periodic wind stress the appearance and disappearance of the pat-

terns are repeated and the upwind flow accordingly varies with phase delay, mostly intensifying near the time when the wind forcing is approximately near the middle of the decaying stage.

Oceanic flow alone little penetrates into the Yellow Sea unless the quadratic bottom friction is used. It is seen that the quadratic bottom friction has a tendency of overestimating the intensity of the upwind flow and the northern extent of penetration into the YS. In the study area strong tidal currents are omnipresent. It is therefore emphasized that proper use of the bottom friction is essential to the successful reproduction of oceanic currents and the upwind flow; use of the quadratic friction as in Wang and Yuan (1988), neglecting tidal motion, can give rise to erroneous or unrealistic results.

A close examination reveals that the presence of oceanic flow sweeping the ECS shelf mainly alters the north-south gradient of sea surface elevation. However, the change is significantly large only near the northern part of E1. Consequently, the intensity and direction of the upwind flow and the southward wind-driven currents on both Chinese and Korean coasts is changed very marginally; noticeable changes are found in the wind-induced flows south of Korean Peninsula. The wind-induced mean upwind flow in the YS deduced by taking into account the interaction with oceanic flow is maintained by the volume supply from relatively strong westward flows on the northen part of E1, that is, near Cheju Island, while the wind-induced mean upwind flow in the YS obtained by neglecting the interaction with oceanic flow is maintained by the volume supply from the whole part of E1.

Although more insight has been in this study attained on the role of the oceanic currents and bottom friction, it however appears that the model response might be dependent upon the open boundary location and bottom topography. For example, in this study the slopes of sea surface elevation along the open boundary are assumed to be constant, which is in reality not true. In addition, it has been found, in the course of defining the open boundary condition, that the shape of deep sea regions representing Okinawa Trough significantly affects the sea surface elevation. We also noted that the incorporation of the northern YS and Bohai Sea is important with regards to the upwind flow. Care must be therefore taken in designing the idealized basin. Extension of the open boundary to the east might be better. Furthermore, the combined effects of the Kuroshio main stream and Taiwan Warm Current might be important. These study will be followed in the future.

ACKNOWLEDGEMENTS

The financial supports from the Ministry of Science and Technology, Korea through the projects PN42800 and PN0145300 are greatly appreciated. Authors are grateful to careful reading and helpful comments made by Dr. C.H. Kim in KORDI, Professor Y.H. Seung Inha University and Professor S.H. Lee Kunsan University.

REFERENCES

Bowden, K.F., 1983. Physical Oceanography of coastal waters, Ellis Horwood Ltd., pp. 320.

Choi, B.H., 1982. Note on currents driven by a steady uniform wind stress on the Yellow Sea and the East China Sea, *La mer*, **20**: 65–74.

Choi, B.H. and K.S. Suh, 1992. Computations of meteorologically induced circulation on the East China Sea using a fine grid three-dimensional numerical model, *J. Korean Soc. Coastal Ocean Engr.*, **4**, **1**: 45–58.

Flather, R.A., 1976. A tidal model of the northwest European continental shelf, *Memories de la Societe Royale des Science de Liege*, **10**: 141–164.

Hannah, C., 1992. Geostrophic control with wind forcing: application to Bass Strait, *J. Phys. Oceanogr.*, **22**: 1596–1599.

Hayashi, T., D.A., Greenberg and C.J.R. Garrett, 1986. Open boundary conditions for numerical models of shelf sea circulation, *Cont. Shelf Res.*, **5**, **4**: 487–497.

Hsueh, Y., 1988. Recent current observations in the eastern Yellow Sea, *J. Geophys. Res.*, **93**: 6875–6884.

Hsueh, Y., 1986. Wintertime winds and coastal sea-level fluctuations in the northeast China Sea. Part II: Numerical model, *J. Phys. Oceanogr.*, **16**: 241–261.

Hsueh, Y. and I.-C., Pang, 1989. Coastally trapped long waves in the Yellow Sea, *J. Phys. Oceanogr.*, **19**: 612–625.

Hunter, J.R., A note on quadratic friction in the presence of tides, *Estuarine and Coastal Marine Sci.*, **3**: 473–475.

Jung, K.T., H.W. Kang, J.K. So and H.J. Lee, 2001. A model-generated circulation in the Yellow Sea and the East China Sea: I. Depth-mean flow fields, *Ocean and Polar Res.*, **23**, 3: 223–242.

Ladner, R.W. and S. Das, 1991. On the computation of flows driven by density gradient: residual currents in the Arabian Gulf, *Appl. Math. Modelling*, **15**: 282–294.

Lee, J.C., 1995. Development of a turbulence closure model for the barotropic shallow seas and its application to the wind-driven circulation of the Yellow Sea and the East China Sea, Ph.D thesis, Sungkyunkwan Univ., pp. 241.

Lee, H.J., K.T. Jung, M.G.G. Foreman and J.Y. Chung, 2000. A three-dimensional mixed Galerkin function model for the oceanic circulation in the Yellow Sea and the East China Sea, *Cont. Shelf Res.*, **20**: 863–895.

Mellor, G.L., 1998. Users guide for a three-dimensional primitive equation, numerical model, pp. 41.

Palma, E.D. and R.P. Matano, 1998. On the implementation of passive open boundary conditions for a general circulation model: The barotropic mode, *J. Geophys. Res.*, **103**, C1: 1319–1341.

Park, Y.H., 1986. A simple theoretical model for the upwind flow

in the southern Yellow Sea, *J. Korean Soc. Oceanogr.*, **21**: 203–210.

Seung, Y.H., 1995. Effect of Shandong Peninsula on the development of mean upwind flow in the Yellow Sea, *J. Korean Soc. Oceanogr.*, **30**, **6**: 537–542.

Takahashi, S., Y. Isoda, and T. Yanagi, 1995. A numerical study on the formation and variation of a clockwise-circulation during winter in the Yellow Sea, *J. Oceanogr.*, **51**: 83–98.

Wang, J. and Y. Yuan, 1988. Numerical modelling of wintertime circulation in the East China Sea, Chinese J. Oceanol. and Limnol., **6**, 4: 300–319.

Wright, D.G., D.A. Greenberg, J.W. Loder and P.C. Smith, 1986. The steady- state barotropic response of the Gulf of Maine and adjacent regions, *J. Phys. Oceanogr.*, **16**: 948–960.

Manuscript received March 5, 2002
Revision accepted July 18, 2002
Editorial handling: Sang-Ho Lee